

# Relativistic Radiation Hydrodynamical Accretion Disk Winds

Jun FUKUE and Chizuru AKIZUKI \*

*Astronomical Institute, Osaka Kyoiku University, Asahigaoka, Kashiwara, Osaka 582-8582*  
fukue@cc.osaka-kyoiku.ac.jp

(Received 0 0; accepted 0 0)

## Abstract

Accretion disk winds blowing off perpendicular to a luminous disk are examined in the framework of fully special relativistic radiation hydrodynamics. The wind is assumed to be steady, vertical, and isothermal. Using a velocity-dependent variable Eddington factor, we can solve the rigorous equations of relativistic radiative hydrodynamics, and can obtain radiatively driven winds accelerated up to the *relativistic* speed. For less luminous cases, disk winds are transonic types passing through saddle type critical points, and the final speed of winds increases as the disk flux and/or the isothermal sound speed increase. For luminous cases, on the other hand, disk winds are always supersonic, since critical points disappear due to the characteristic nature of the disk gravitational fields. The boundary between the transonic and supersonic types is located at around  $\hat{F}_c \sim 0.1(\varepsilon + p)/(\rho c^2)/\gamma_c$ , where  $\hat{F}_c$  is the radiative flux at the critical point normalized by the local Eddington luminosity,  $(\varepsilon + p)/(\rho c^2)$  is the enthalpy of the gas divided by the rest mass energy, and  $\gamma_c$  is the Lorentz factor of the wind velocity at the critical point. In the transonic winds, the final speed becomes 0.4–0.8*c* for typical parameters, while it can reach  $\sim c$  in the supersonic winds.

**Key words:** accretion, accretion disks — astrophysical jets — gamma-ray burst — radiative transfer — relativity

## 1. Introduction

Mass outflows – accretion disk winds – from a luminous disk are observed in various active objects, such as cataclysmic variables (CVs), supersoft X-ray sources (SSXSs), microquasars ( $\mu$ QSOs), broad absorption line quasars (BAL QSOs), and so on. Radiatively driven wind emanating from an accretion disk is a clue to the formation mechanism of astrophysical jets and winds in these objects (see Kato et al. 1998, 2007 for a review of accretion disks).

So far, radiatively driven outflows from a luminous disk have been extensively studied by many researchers (Bisnovatyi-Kogan, Blinnikov 1977; Katz 1980; Icke 1980; Melia, Königl 1989; Misra, Melia 1993; Tajima, Fukue 1996, 1998; Watarai, Fukue 1999; Hirai, Fukue 2001; Fukue et al. 2001; Orihara, Fukue 2003), and by numerical simulations (Eggum et al. 1985, 1988; Kley 1989; Okuda et al. 1997; Kley, Lin 1999; Okuda, Fujita 2000; Okuda 2002; Okuda et al. 2005; Ohsuga et al. 2005; Ohsuga 2006). In almost all of these studies, however, the luminous disk was treated as an external radiation source (optically thin approximation), and the radiation transfer in the flow was not solved. Although radiation hydrodynamical equations were solved in the numerical simulations, the methods were rather limited; e.g., the equilibrium between gas and radiation was assumed, the flux-limited diffusion approximation was adopted, the flow velocity was

subrelativistic on the order of 0.1*c*, or the optically thick to thin transition was not properly treated. Up to now, in relation to accretion disk winds no one solved the fully relativistic radiation hydrodynamical equations.

Recently, radiation hydrodynamical mass outflows have been examined for the first time in the fully relativistic cases for the plane-parallel case (Fukue 2005, 2006; Fukue, Akizuki 2006; see also Akizuki and Fukue 2007 for the spherical case). In these studies, however, the gas pressure was ignored for simplicity, although the relativistic radiation hydrodynamical equations were solved. In this paper, we thus take into account the gas pressure, and obtain the relativistic radiation hydrodynamical *winds* blowing off from a luminous flat disk within the framework of a fully special relativistic regime.

In the next section we describe the basic equations in the vertical direction, and examine critical points. In section 3 we obtain transonic winds as well as supersonic ones. The final section is devoted to concluding remarks.

## 2. Basic Equations and Boundary Conditions

Let us suppose a luminous flat disk, inside of which gravitational or nuclear energy is released via viscous heating or other processes. The radiation energy is transported in the vertical direction, and the disk gas, itself, also moves in the vertical direction due to the action of radiation pressure (steady plane-parallel approximation). We do not consider the rotation of the gas. As for the order of the flow velocity *v*, we consider the fully relativistic regime, where the terms are retained up to the second or-

\* Present address: Center for Computational Physics, University of Tsukuba, Tennoudai 1-1-1, Tsukuba, Ibaraki, 305-8577

der of  $(v/c)$ . As for the gravity, on the other hand, we adopt the pseudo-Newtonian approximation (Paczynski, Wiita 1980), since we do not consider the region very close to the Schwarzschild radius. For simplicity, in the present paper, we assume that the gas is *isothermal*, because we focus our attention on the general properties of transonic disk winds driven by disk radiation fields under relativistic radiation hydrodynamics. We further assume the radiative equilibrium and use the gray approximation. Finally, in order to close moment equations, we adopt the *velocity-dependent variable Eddington factor* proposed by Fukue (2006).

### 2.1. Basic Equations

Under these assumptions, the radiation hydrodynamic equations for steady vertical ( $z$ ) winds are described as follows (Kato et al. 1998, 2007; Fukue 2006).

The continuity equation is

$$\rho c u = J \quad (= \text{const.}), \quad (1)$$

where  $\rho$  is the proper gas density,  $u$  the vertical four velocity,  $J$  the mass-loss rate per unit area, and  $c$  the speed of light. The four velocity  $u$  is related to the proper three velocity  $v$  by  $u = \gamma v/c$ , where  $\gamma$  is the Lorentz factor,  $\gamma = \sqrt{1 + u^2} = 1/\sqrt{1 - (v/c)^2}$ .

The equation of motion is, within the present approximation,

$$\begin{aligned} c^2 u \frac{du}{dz} = & -\frac{GMz}{(R - r_g)^2 R} - \gamma^2 \frac{c^2}{\varepsilon + p} \frac{dp}{dz} \\ & + \frac{\rho c^2}{\varepsilon + p} \frac{\kappa_{\text{abs}} + \kappa_{\text{sca}}}{c} \\ & \times [F\gamma(1 + 2u^2) - (cE + cP)\gamma^2 u], \end{aligned} \quad (2)$$

where  $M$  is the mass of the central object,  $R = \sqrt{r^2 + z^2}$ ,  $r$  being the radius,  $r_g (= 2GM/c^2)$  the Schwarzschild radius,  $\varepsilon$  the gas internal energy per unit proper volume,  $p$  the gas pressure measured in the comoving frame,  $\kappa_{\text{abs}}$  and  $\kappa_{\text{sca}}$  the absorption and scattering opacities (gray), defined in the comoving frame,  $E$  the radiation energy density,  $F$  the radiative flux, and  $P$  the radiation pressure observed in the inertial frame (Fukue 2006; Kato et al. 2007). The first term in the square bracket on the right-hand side of equation (2) means the radiatively-driven force, which is modified to the order of  $u^2$ , whereas the second term is the radiation drag force, which is also modified, but roughly proportional to the velocity. Compared with the previous researches (Fukue 2006; Fukue and Akizuki 2006), we have added the pressure gradient force, the second term on the right-hand side of equation (2), and the related factor,  $\rho c^2/(\varepsilon + p)$  to the third term.

The radiative equilibrium condition is, in the inertial frame, written as

$$0 = j - \kappa_{\text{abs}} c E \gamma^2 - \kappa_{\text{abs}} c P u^2 + 2\kappa_{\text{abs}} F \gamma u, \quad (3)$$

where  $j$  is the emissivity defined in the comoving frame (Fukue 2006; Kato et al. 2007).

For radiation fields, the zeroth-moment equation becomes

$$\begin{aligned} \frac{dF}{dz} = & \rho \gamma [j - \kappa_{\text{abs}} c E + \kappa_{\text{sca}} (cE + cP) u^2 \\ & + \kappa_{\text{abs}} F u / \gamma - \kappa_{\text{sca}} F (1 + v^2/c^2) \gamma u] \\ = & -\rho (\kappa_{\text{abs}} + \kappa_{\text{sca}}) \frac{u}{\gamma} \\ & \times [F(1 + 2u^2)\gamma - (cE + cP)\gamma^2 u], \end{aligned} \quad (4)$$

where we use equation (3) for the second equality. The first-moment equation is

$$\begin{aligned} \frac{dP}{dz} = & \frac{\rho \gamma}{c} [j(u/\gamma) - \kappa_{\text{abs}} F + \kappa_{\text{abs}} c P (u/\gamma) \\ & - \kappa_{\text{sca}} F (1 + 2u^2) + \kappa_{\text{sca}} (cE + cP) \gamma u] \\ = & -\rho (\kappa_{\text{abs}} + \kappa_{\text{sca}}) \frac{1}{c} \\ & \times [F(1 + 2u^2)\gamma - (cE + cP)\gamma^2 u], \end{aligned} \quad (5)$$

where we use equation (3) for the second equality (Fukue 2006; Kato et al. 2007).

In order to close moment equations for radiation fields, we need some closure relation. Instead of the usual Eddington approximation, we here adopt a *velocity-dependent variable Eddington factor*  $f(\beta)$ ,

$$P_0 = f(\beta) E_0 \quad (6)$$

in the comoving frame, where  $P_0$  and  $E_0$  are the quantities in the comoving frame, and  $\beta = v/c$ . If we adopt this form (6) as the closure relation in the comoving frame, the transformed closure relation in the inertial frame is

$$cP(1 + u^2 - f u^2) = cE(f\gamma^2 - u^2) + 2F\gamma u(1 - f), \quad (7)$$

or equivalently,

$$cP(1 - f\beta^2) = cE(f - \beta^2) + 2F\beta(1 - f). \quad (8)$$

As a form of the function  $f(\beta)$ , we adopt the simplest one:

$$f(\beta) = \frac{1}{3} + \frac{2}{3}\beta \quad (9)$$

for a plane-parallel geometry (Fukue 2006; Fukue, Akizuki 2006; cf. Akizuki and Fukue 2007 for a spherically symmetric geometry).

Using continuity equation (1) and equation of motion (2), after some manipulations, we obtain the so-called *wind equation*,

$$\begin{aligned} \frac{du}{dz} = & \frac{u}{\gamma^2(v^2 - c_T^2)} \left\{ -\frac{GMz}{(R - r_g)^2 R} \right. \\ & + \frac{\rho c^2}{\varepsilon + p} \frac{\kappa_{\text{abs}} + \kappa_{\text{sca}}}{c} \\ & \left. \times [F\gamma(1 + 2u^2) - (cE + cP)\gamma^2 u] \right\}, \end{aligned} \quad (10)$$

or equivalently,

$$\begin{aligned} \frac{dv}{dz} = & \frac{v}{\gamma^4(v^2 - c_T^2)} \left\{ -\frac{GMz}{(R - r_g)^2 R} \right. \\ & + \delta^2 \frac{\kappa_{\text{abs}} + \kappa_{\text{sca}}}{c} \\ & \left. \times \gamma^3 \left[ F\gamma \left( 1 + \frac{v^2}{c^2} \right) - (cE + cP) \frac{v}{c} \right] \right\}. \end{aligned} \quad (11)$$

Here,  $c_T$  is the constant isothermal sound speed, defined by

$$c_T^2 \equiv \frac{c^2 p}{\varepsilon + p} \quad (\text{const.}). \quad (12)$$

Under the present isothermal assumption, the factor,

$$\delta^2 \equiv \frac{\rho c^2}{\varepsilon + p} \quad (\text{const.}), \quad (13)$$

is also a constant parameter.

Eliminating  $\rho$  and  $E$  with the help of equations (1) and (7), equations (11), (4), and (5) become

$$\frac{dv}{dz} = \frac{v}{\gamma^4(v^2 - c_T^2)} \left[ -\frac{GMz}{(R - r_g)^2 R} + \delta^2 \frac{\kappa_{\text{abs}} + \kappa_{\text{sca}}}{c} \times \gamma \frac{F(f + \beta^2) - cP(1 + f)\beta}{f - \beta^2} \right], \quad (14)$$

$$\frac{dF}{dz} = -J \frac{\kappa_{\text{abs}} + \kappa_{\text{sca}}}{c} \frac{F(f + \beta^2) - cP(1 + f)\beta}{f - \beta^2}, \quad (15)$$

$$c \frac{dP}{dz} = -\frac{J}{u} \frac{\kappa_{\text{abs}} + \kappa_{\text{sca}}}{c} \gamma \frac{F(f + \beta^2) - cP(1 + f)\beta}{f - \beta^2}. \quad (16)$$

For the optical depth  $\tau$ , defined by  $d\tau \equiv -(\kappa_{\text{abs}} + \kappa_{\text{sca}})\rho dz$ , we have

$$\frac{d\tau}{dz} = -J \frac{\kappa_{\text{abs}} + \kappa_{\text{sca}}}{c} \frac{1}{u}. \quad (17)$$

Finally, using the nondimensional variables, such as  $\hat{z} = z/r_g$ ,  $\beta = v/c$ ,  $\hat{F} = F/[L_E/(4\pi r_g^2)]$ ,  $\hat{P} = cP/[L_E/(4\pi r_g^2)]$ , where  $L_E [= 4\pi cGM/(\kappa_{\text{abs}} + \kappa_{\text{sca}})]$  is the Eddington luminosity, basic equations (14)–(17) are normalized as

$$\frac{d\beta}{dz} = \frac{\beta}{\gamma^4(\beta^2 - \hat{c}_T^2)} \times \left[ -\frac{\hat{z}}{2(\hat{R} - 1)^2 \hat{R}} + \frac{\delta^2 \gamma \hat{F}(f + \beta^2) - \hat{P}(1 + f)\beta}{2(f - \beta^2)} \right] \quad (18)$$

$$\frac{d\hat{F}}{d\hat{z}} = -\frac{\hat{J} \hat{F}(f + \beta^2) - \hat{P}(1 + f)\beta}{2(f - \beta^2)}, \quad (19)$$

$$\frac{d\hat{P}}{d\hat{z}} = -\frac{\hat{J} \hat{F}(f + \beta^2) - \hat{P}(1 + f)\beta}{2\beta(f - \beta^2)} \quad (20)$$

$$\frac{d\tau}{d\hat{z}} = -\frac{\hat{J}}{2\gamma\beta}, \quad (21)$$

where  $\hat{c}_T^2 = c_T^2/c^2 = p/(\varepsilon + p)$ ,  $\delta^2 = \rho c^2/(\varepsilon + p)$ , and  $\hat{J} = c^2 J/[L_E/(4\pi r_g^2)]$ .

We solve equations (18)–(21) under regularity conditions at the sonic point and appropriate boundary conditions at the moving surface with a variable Eddington factor (9).

## 2.2. Regularity Conditions and Boundary Conditions

As is well known, equation (18) has critical points, where the denominator and numerator vanish, simultaneously. Hence, transonic solutions, which passes through

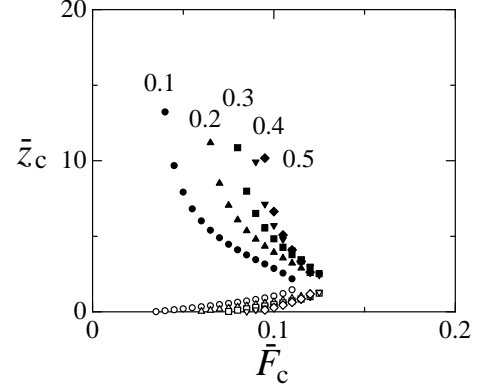


**Fig. 1.** Loci and types of critical points as a function of the radiative flux  $\hat{F}_c$  at the critical point for several values of the isothermal sound speed  $\hat{c}_T$ . Filled symbols represent the saddle type, whereas open symbols denote the center type. The values of  $\hat{c}_T$  are attached on each symbols. The other parameters are fixed as  $\delta = 1$ ,  $\tau_c = 1$ , and  $\hat{P}_c = 0.1$ .

critical points, satisfy the *regularity conditions* at the critical point. In order to obtain transonic wind solutions, in this paper, we first search the location of critical points, examine the types of critical points, and calculate the transonic solutions from the critical point both inward and outward directions.

In contrast to a simple spherical flow under the gravity of the central object, the gravitational field of the disk wind does not monotonically decrease, but increases at first and then decreases (Fukue 2002). As a result, there may appear multiple critical points. In figure 1, we show some typical examples.

In figure 1, the height  $\hat{z}_c$  of critical points are plotted as a function of the radiative flux  $\hat{F}_c$  at the critical point for several values of the isothermal sound speed  $\hat{c}_T$ . Filled symbols represent the saddle type, through which physical solutions can path, whereas open symbols denote the center type, where no solution can path (Kato et al. 2007). The values of  $\hat{c}_T$  are attached on each symbols. The other parameters are fixed as  $\delta = 1$ ,  $\tau_c = 1$ , and  $\hat{P}_c = 0.1$ .

As is easily seen in figure 1, in less-luminous cases there appear two positions for the same values of  $\hat{F}_c$ . Of these, the upper point is usually a saddle type, whereas the lower one is a center type. On the other hand, in luminous cases there is no critical point. Roughly speaking, two critical points exist when  $\delta^2 \gamma_c \hat{F}_c < 0.1$ , or

$$\frac{F_c}{L_E/(4\pi r_g^2)} < 0.1 \frac{\varepsilon + p}{\rho c^2} \frac{1}{\gamma_c}, \quad (22)$$

where  $F_c$  is the radiative flux at the critical point,  $(\varepsilon + p)/(\rho c^2)$  is the enthalpy of the gas divided by the rest mass energy, and  $\gamma_c$  is the Lorentz factor of the wind velocity at the critical point.

In addition to the above regularity conditions, at the wind top of  $\tau = 0$  we must impose the boundary conditions, which is different from the usual ones for a static photosphere, since the wind top moves upward at a rel-

ativistic speed (Fukue 2005). In the case of a “moving photosphere”, due to relativistic aberration and Doppler effect (cf. Fukue 2000), the boundary conditions imposed for the radiation quantities become

$$\frac{cP_s}{F_s} = \frac{2 + 6\beta_s + 6\beta_s^2}{3 + 8\beta_s + 3\beta_s^2}, \quad (23)$$

where the subscript ‘s’ denotes the quantities at the wind top, and  $\beta_s$  is a final speed at the wind top.

### 3. Relativistic Accretion Disk Winds

In this section we show typical solutions of relativistic radiation hydrodynamical accretion disk winds for transonic and supersonic cases.

In order to obtain a transonic solution, by numerically solving equations (18)–(21), we must specify the initial values of  $r$ , and  $z_c$ ,  $\beta_c$ ,  $F_c$ ,  $P_c$ ,  $\tau_c$  at the critical point for a given set of parameters of  $c_T$ ,  $\delta$ , and  $J$ . However, there are three restrictive conditions; two regularity conditions at the critical points, and one boundary condition at the wind top. Hence, we have six freedoms. In order to see the effect of the radiative force and the gas pressure, in the present paper we set  $\hat{r} = 3$ ,  $\tau_c = 1$ ,  $\delta = 1$ , and  $\hat{J} = 0.1$ . If we give the values of  $F_c$  and  $c_T$ , the values of  $z_c$ ,  $\beta_c$ , and  $P_c$  are automatically determined.

Several examples of transonic solutions are shown in figure 2. Physical quantities are normalized in terms of the speed of light  $c$ , the Schwarzschild radius  $r_g$ , and the Eddington luminosity  $L_E$  [ $= 4\pi cGM/(\kappa_{\text{abs}} + \kappa_{\text{sca}})$ ]; the units of  $F$  and  $cP$  are  $L_E/(4\pi r_g^2)$ .

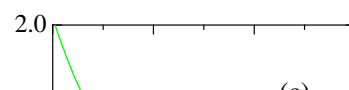
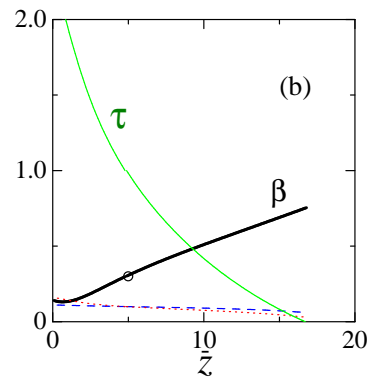
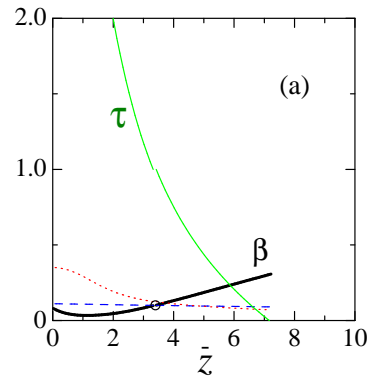
In figure 2 we show the flow velocity  $\beta$  (thick solid curve), the radiative flux  $\hat{F}$  (dashed one), the radiation pressure  $\hat{P}$  (dotted one), and the optical depth  $\tau$  (solid curve), as a function of the height  $\hat{z}$  for  $\hat{r} = 3$ ,  $\delta = 1$ ,  $\tau_c = 1$ ,  $\hat{F}_c = 1$ ,  $\hat{J} = 0.1$ , and  $\hat{c}_T = 0.1, 0.3, 0.5$ . Critical points are marked by open circles.

As is seen in, e.g., figure 2a, the wind velocity slightly decreases at first, because of the existence of the center-type critical point, then increases to pass through the saddle-type critical point, and finally reaches the final speed at the wind top of  $\tau = 0$ . The radiative flux  $F$  slightly decreases, as the height increases. In the relativistic radiation flow, the radiative flux does not conserve, but decreases, since the radiation field acts to accelerate the gas. As for the effect of the gas pressure, the velocity fields entirely increase as the isothermal sound speed increases.

The effects of the radiation force and gas pressure on the acceleration of winds are summarized in figures 3 and 4.

In figure 3 we show the wind final velocity  $\beta_s$  (thick solid curve), the heights,  $\hat{z}_s$  and  $\hat{z}_c$ , of the wind top and the critical point (dashed ones), and the radiation pressure  $\hat{P}_c$  at the critical point (dotted one), as a function of the radiative flux  $\hat{F}_c$  at the critical point. The other parameters are fixed as  $\hat{r} = 3$ ,  $\delta = 1$ ,  $\tau_c = 1$ ,  $\hat{J} = 0.1$ , and  $\hat{c}_T = 0.3$ .

As is seen in figure 3, the wind final velocity increases



with  $\hat{F}_c$ . The Lorentz factor  $\gamma_s$  of the wind final velocity is well fitted by

$$\gamma_s \sim 1.07 + 1.50\hat{F}_c. \quad (24)$$

Roughly speaking, this is understood as follows. In the present treatment under special relativity and pseudo-Newtonian potential, there is no rigorous energy integral. However, the pseudo total energy along the wind,

$$Jc^2 \frac{\varepsilon + p}{\rho c^2} \gamma \left[ 1 - \frac{r_g}{2(R - r_g)} \right] + F, \quad (25)$$

is approximately conserved within the error of 10%. If we denote the gravitational potential by  $\phi$ , this pseudo energy conservation is written in the non-dimensional form as

$$\frac{\hat{J}}{\delta^2} \gamma(1 + \hat{\phi}) + \hat{F} = \text{const.}, \quad (26)$$

or

$$\frac{\hat{J}}{\delta^2} \gamma(1 + \hat{\phi}) + \hat{F} \Big|_s = \frac{\hat{J}}{\delta^2} \gamma(1 + \hat{\phi}) + \hat{F} \Big|_c. \quad (27)$$

Hence, in general  $\gamma_s$  linearly depends on  $\hat{F}_c$ .

In figure 4 we show the wind velocity  $\beta_s$  (thick solid curve), the heights,  $\hat{z}_s$  and  $\hat{z}_c$ , of the wind top and the critical point (dashed ones), and the radiation pressure  $\hat{P}_c$  at the critical point (dotted one), as a function of the isothermal sound speed  $\hat{c}_T$ . The other parameters are fixed as  $\hat{r} = 3$ ,  $\delta = 1$ ,  $\tau_c = 1$ ,  $\hat{J} = 0.1$ , and  $\hat{F}_c = 0.1$ .

As is seen in figure 4, the wind final velocity increases with  $\hat{c}_T$ . The Lorentz factor  $\gamma_s$  is now fitted by

$$\gamma_s \sim 1 + 0.3\hat{c}_T + 1.3\hat{c}_T^2. \quad (28)$$

This is also understood by a rough energy conservation discussed above. In this case,  $\gamma_s$  linearly depends on  $\gamma_c$ , and  $\gamma_c = 1/\sqrt{1 - \hat{c}_T^2}$ , therefore there appears  $\hat{c}_T^2$  term.

In addition to transonic solutions, an example of supersonic solutions is shown in figure 5. In figure 5 we show the flow velocity  $\beta$  (thick solid curve), the radiative flux  $\hat{F}$  (dashed one), the radiation pressure  $\hat{P}$  (dotted one), and the optical depth  $\tau$  (solid curve), as a function of the height  $z$  for  $\hat{r} = 3$ ,  $\delta = 1$ ,  $\tau_0 = 2$ ,  $\hat{F}_0 = 1$ ,  $\beta_0 = 0.6$ ,  $\hat{c}_T = 0.57$ , and  $\hat{J} = 0.1$ , where the subscript 0 means the values at  $z = 0$ .

In this example of supersonic winds, the wind final speed is almost the speed of light, since both the initial flux and isothermal sound speed are large.

#### 4. Concluding Remarks

In this paper we have examined the relativistic radiation hydrodynamical winds from a luminous accretion disk in the relativistic regime of  $(v/c)^2$ . The wind is assumed to be steady, vertical, and isothermal. Using a velocity-dependent variable Eddington factor, the basic equations can be numerically solved without meeting the pathological singular point at  $v = c/\sqrt{3}$  to reach the relativistic regime.

For less luminous cases, vertical disk winds are transonic types passing through saddle-type critical points,

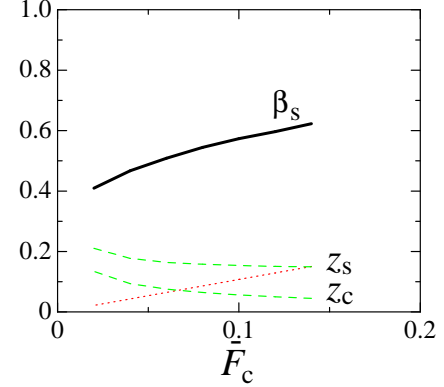


**Fig. 3.** Wind final velocity  $\beta_s$  at the wind top (thick solid curve), heights,  $\hat{z}_s$  and  $\hat{z}_c$ , of the wind top and the critical point (dashed ones), and radiation pressure  $\hat{P}_c$  at the critical point (dotted one), as a function of the radiative flux  $\hat{F}_c$  at the critical point. For heights,  $\hat{z}/100$  is plotted. The parameters are  $\hat{r} = 3$ ,  $\delta = 1$ ,  $\tau_c = 1$ ,  $\hat{J} = 0.1$ , and  $\hat{c}_T = 0.3$ .

and the wind final speeds are 0.4–0.8  $c$  for typical parameters. For luminous cases, on the other hand, disk winds become supersonic types without passing through any critical points, and the wind final speeds becomes on the order of  $c$ . The boundary between the transonic and supersonic types is located at around  $\hat{F}_c \sim 0.1(\varepsilon + p)/(\rho c^2)/\gamma_c$ .

In usual standard accretion disks, the local luminosity is sub-Eddington. Hence, for proton-electron normal plasmas the above condition is sufficiently fulfilled, and transonic winds driven by radiation and gas pressures would blow off. For electron-positron pair plasmas, on the other hand, the local luminosity becomes super-Eddington, and pair winds would supersonically blow off.

The maximum attainable velocity of the wind can be roughly estimated by the energy conservation. In the Schwarzschild space-time, without any energy source except for gravity, the total energy of the radiation hydrodynamical flow along the streamline,

$$Jc^2 \frac{\varepsilon + p}{\rho c^2} \gamma \sqrt{g_{00}} + g_{00} F = \dot{E} \quad (\text{const.}), \quad (29)$$

where  $g_{00} = \sqrt{1 - r_g/R}$ , is conserved. If all of the thermal

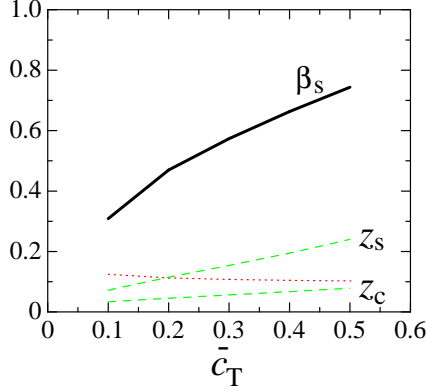


**Fig. 4.** Wind final velocity  $\beta_s$  at the wind top (thick solid curve), heights,  $\hat{z}_s$  and  $\hat{z}_c$ , of the wind top and the critical point (dashed ones), and radiation pressure  $\hat{P}_c$  at the critical point (dotted one), as a function of the isothermal sound speed  $\hat{c}_T$ . For heights,  $\hat{z}/100$  is plotted. The parameters are  $\hat{r} = 3$ ,  $\delta = 1$ ,  $\tau_c = 1$ ,  $\hat{J} = 0.1$ , and  $\hat{F}_c = 0.1$ .

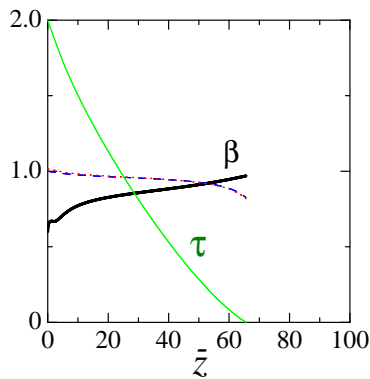


**Fig. 5.** Flow velocity  $\beta$  (thick solid curve), radiative flux  $\hat{F}$  (dashed one), radiation pressure  $\hat{P}$  (dotted one), and optical depth  $\tau$  (solid green curve), as a function of the height  $\hat{z}$ . The parameters are  $\hat{r} = 3$ ,  $\delta = 1$ ,  $\tau_0 = 2$ ,  $\hat{F}_0 = 1$ ,  $\beta_0 = 0.6$ ,  $\hat{c}_T = 0.57$  and  $\hat{J} = 0.1$ .

energy of the gas and the radiative energy in the initial state is converted to the bulk energy of the gas, the final velocity would become its upper limit:

$$Jc^2\gamma_\infty = Jc^2\frac{\varepsilon+p}{\rho c^2}\gamma\sqrt{g_{00}} + g_{00}F\Big|_{z=0}. \quad (30)$$

If, further, the gas is at rest in the initial state and in the virial state,  $[(\varepsilon+p)/(\rho c^2)]\sqrt{g_{00}}|_{z=0} = 1$ , then we finally have the maximum attainable velocity as

$$\gamma_\infty = 1 + \frac{g_{00}F|_0}{Jc^2} = 1 + \left(1 - \frac{1}{\hat{r}}\right)\frac{\hat{F}_0}{\hat{J}}. \quad (31)$$

For example, in the present typical case of  $\hat{r} = 3$ ,  $\hat{F} \sim 0.1$ ,  $\hat{J} = 0.1$ , we have  $\gamma_\infty = 1.666$ , or  $\beta_\infty = 0.8$ .

Hence, from the view point of energetics, the final velocity becomes higher and higher, as the ratio  $\hat{F}_0/\hat{J}$  becomes large; the radiative flux is so high or the mass-loss rate is so low. In other words, if the small amount of the gas gains the large amount of the radiation energy, the final bulk velocity becomes high. In general, however, it may be difficult for such a re-distribution of energy to take place, and the ratio  $\hat{F}_0/\hat{J}$  would be on the order of unity.

Thus, we conclude that the maximum attainable velocity of accretion disk winds emanating from the disk inner region would be  $0.8c$  or so, as long as it consists of normal plasmas. This conclusion is consistent with the current theoretical works referred in the introduction, those explain mildly relativistic jets of  $0.26c$  ( $\gamma = 1.04$ ) in SS 433 to highly relativistic jets of  $0.92c$  ( $\gamma = 2.55$ ) in several microquasars.

For ultra-relativistic jets of  $0.99c$  ( $\gamma = 10$ ) supposed in several active galactic nuclei or extremely relativistic jets of  $0.9999c$  ( $\gamma = 100$ ) expected to gamma-ray bursts, it may be necessary some other processes, including an extraordinary re-distribution of energy, pair dominant plasmas, an energy deposition from other energy sources, such as a nuclear one via neutrino, and so on.

This work has been supported in part by a Grant-in-Aid for the Scientific Research (18540240 J.F.) of the Ministry of Education, Culture, Sports, Science and Technology.

## References

- Akizuki, C., & Fukue, J. 2007, PASJ submitted  
 Bisnovatyi-Kogan, G. S., & Blinnikov, S. I. 1977, A&A, 59, 111  
 Eggum, G. E., Coroniti, F. V., & Katz, J. I. 1985, ApJ, 298, L41  
 Eggum, G. E., Coroniti, F. V., & Katz, J. I. 1988, ApJ, 330, 142  
 Fukue, J. 2000, PASJ, 52, 829  
 Fukue, J. 2002, PASJ, 54, 415  
 Fukue, J. 2005, PASJ, 57, 1023  
 Fukue, J. 2006, PASJ, 58, 461  
 Fukue, J., & Akizuki, C. 2006, PASJ, 58, 1073  
 Fukue, J., Tojyo, M., & Hirai, Y. 2001, PASJ, 53, 555  
 Hirai, Y., & Fukue, J. 2001, PASJ, 53, 285  
 Icke, V. 1980, AJ, 85, 329

- Kato, S., Fukue, J., & Mineshige, S. 1998, *Black-Hole Accretion Disks* (Kyoto: Kyoto University Press)
- Kato, S., Fukue, J., & Mineshige, S. 2007, *Black-Hole Accretion Disks: New Paradigm* (Kyoto: Kyoto University Press)
- Katz, J. I. 1980, *ApJ*, 236, L127
- Kley, W. 1989, *A&A*, 222, 141
- Kley, W., & Lin, D.N.C. 1999, *ApJ*, 518, 833
- Melia, F., & Königl, A. 1989, *ApJ*, 340, 162
- Misra, R., & Melia, F. 1993, *ApJ*, 419, L25
- Okuda, T. 2002, *PASJ*, 54, 253
- Okuda, T., & Fujita, M. 2000, *PASJ*, 52, L5
- Okuda, T., Fujita, M., & Sakashita, S. 1997, *PASJ*, 49, 679
- Okuda, T., Teresi, V., Toscano, E., & Molteni, D. 2005, *MNRAS*, 357, 295
- Ohsuga, K. 2006, *ApJ*, 640, 923
- Ohsuga, K., Mori, M., Nakamoto, T., & Mineshige, S. 2005, *ApJ*, 628, 368
- Orihara, S., & Fukue, J. 2003, *PASJ*, 55, 953
- Paczyński, B., & Wiita, P. J. 1980, *A&A*, 88, 23
- Tajima, Y., & Fukue, J. 1996, *PASJ*, 48, 529
- Tajima, Y., & Fukue, J. 1998, *PASJ*, 50, 483
- Watarai, K., & Fukue, J. 1999, *PASJ*, 51, 725